Soils and Foundations 2014;54(6):1175–1187

HOSTED BY

ELSEVIER

The Japanese Geotechnical Society

Soils and Foundations

www.sciencedirect.com
journal homepage: www.elsevier.com/locate/sandf

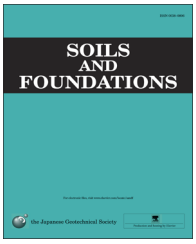

Failure behavior and mechanism of slopes reinforced using soil nail wall under various loading conditions

Ga Zhang*[,1], Jie Cao, Liping Wang

State Key Laboratory of Hydroscience and Engineering, Tsinghua University, Beijing, PR China

Received 26 September 2013; received in revised form 28 July 2014; accepted 7 September 2014
Available online 11 December 2014

Abstract

Soil–nailing technology is widely applied in practice for reinforcing slopes. A series of centrifuge model tests was conducted on slopes reinforced with a soil nail wall under three types of loading conditions. The behavior and mechanism of failure process of the reinforced slopes were studied using image-based observation and displacement measurements for the slope, nails, and cement layer. The nailing significantly increased the stability level and restricted the tension cracks of the slopes. Increasing the nail length improved the stability of the reinforced slopes with deeper slip surfaces. The reinforced slope exhibited a significant failure process, in which slope slippage failure and cement layer fracture occurred in conjunction with a coupling effect. The deformation localization was induced by the loading within the slope and ultimately developed into a slip surface. The nailing reinforced the slope by significantly delaying the occurrence of the deformation localization within the slope. The failure of nails was recognized as a combination of pull-out failure and bend deformation. The loading conditions were shown to have a significant effect on slope deformation and nail deflection, and they consequently influenced the failure behavior and its formation sequence.

Keywords: Slope; Reinforced soils; Soil nailing; Failure; Centrifuge model test

1. Introduction

As soil–nailing technology is increasingly applied to reinforce slopes, the number of studies on the design of nail-reinforced slopes has also increased. The effective designing method depends on the robust evaluation of the stability level of the reinforced slopes, which should be based on a sound understanding of failure behavior and reinforcement mechanisms.

A diverse range of methods have been proposed for analyzing the stability of nail-reinforced slopes, including the limit equilibrium method, the finite-element method, and the kinematics method. Based on the different hypotheses for slope failure surface and/or the soil–nail interaction model, soil nail behavior was analyzed and the design was optimized with respect to various parameters, including length, spacing, inclination, diameter and geometric arrangements (e.g., Shen et al., 1981; Juran et al., 1990; Kim et al., 1997; Yang and Drumm, 2000; Guler and Bozkurt, 2004; Cheuk et al., 2005; Patra and Basudhar, 2005; Gui and Ng, 2006). A non-linear finite element program, PLAXIS, used to analyze the stability level of nail-reinforced slopes has revealed that the optimal nail orientation decreases as the gradient of the slope increases (Fan and Luo, 2008).

The reinforcement effect and mechanism for soil nailing in slopes was investigated via observations of the strain-stress

*Correspondence to: Institute of Geotechnical Engineering, Department of Hydraulic Engineering, Tsinghua University, Beijing 100084, PR China. Tel./fax: +86 10 62795679.
E-mail addresses: zhangga@tsinghua.edu.cn (G. Zhang), caojie.06@gmail.com (J. Cao), wlp04@mails.tsinghua.edu.cn (L. Wang).
[1]Institute of Geotechnical Engineering, Department of Hydraulic Engineering, Tsinghua University, Beijing 100084, PR China.
Peer review under responsibility of The Japanese Geotechnical Society.

http://dx.doi.org/10.1016/j.sandf.2014.11.011
0038-0806/

performance of nails, the safety level of soil nail wall, and the soil–nail interaction (e.g., Wong et al., 1997; Junaideen et al., 2004; Zhou and Yin, 2008; Zhou et al., 2009). The strength reduction method and the limit equilibrium method were utilized to analyze the soil–nail interaction in reinforced slopes and showed that failure modes influence the line of maximum tension (Wei and Cheng, 2010).

Field observation has played an important role in understanding the behavior of slopes reinforced with soil nailing (e.g., Andrzej et al., 1988; Nowatzki and Samtani, 2004). Another study analyzed the response of a full-scale nail-reinforced slope using observed and measured data (Turner and Jensen, 2005). Centrifuge model tests have been effectively used to explore the deformation and failure behavior of nail-reinforced slopes under various loading conditions through producing an equivalent gravity-induced stress field between the model and prototype (e.g., Zornberg et al., 1997; Zhang et al., 2001; Wang et al., 2010). The aseismic nail-reinforcement mechanism was demonstrated by comparing the deformation between reinforced and unreinforced slopes via centrifuge model tests under earthquake conditions (Wang et al., 2010) and 1*g* shaking table tests (Tatsuoka et al., 2012). Zhang et al., (2013) employed centrifuge model tests to analyze the deformation behavior and failure process of a nail-reinforced slope under the surface loading condition, and they illustrated the influence rules of different nail layouts.

The objective of this paper is to investigate the failure mechanism of slopes reinforced with soil nail wall using serialized centrifuge model tests. The steps were as follows: (1) the shotcrete wall and different loading conditions were simulated to systematically understand the actual response of the reinforced slopes; (2) the failure modes were clarified according to the test observations; (3) the slope failure process, together with the fracture and deformation of the reinforcement structures, was captured according to the test observations and measurement results: and (4) the failure and reinforcement mechanisms were elucidated through integrated analysis of the deformation and failure processes, which was accomplished by accurately measuring the displacement of entire slopes.

2. Tests

2.1. Schemes

All centrifuge model tests were conducted using a 50*g*-ton geotechnical centrifuge at Tsinghua University, which has an effective radius of 2 m and a maximum centrifugal acceleration of 250*g*. The deformation and failure processes of nail-reinforced cohesive soil slopes were observed under different loading conditions, including self-weight loading, vertical loading on the top of the slope, and excavation at the toe of the slope (Table 1, Fig. 1).

The slope gradient and nail length were varied to investigate their influence on the response of the reinforced slopes. The gradients of slope for the tests ranged from 1.2:1 to 5:1 (Horizontal:Vertical). Three nail lengths from 4 cm to 8 cm were used in the tests. Unreinforced slopes were also simulated for comparison with the reinforced slopes, to analyze the reinforced mechanism.

Table 1
List of centrifuge model tests.

Loading condition	Gradient (V:H)	Nail length (cm)	No.
Self-weight loading	5:1	8	G5-R8-S
		4	G5-R4-S
		–	G5-U-S
	3:1	8	G3-R8-S
		6	G3-R6-S
		4	G3-R4-S
Excavation	3:1	8	G3-R8-E
	2:1	8	G2-R8-E
		6	G2-R6-E
		4	G2-R4-E
	1.2:1	8	G1.2-R4-E
Vertical loading	3:1	8	G3-R8-L
		6	G3-R6-L
	2:1	6	G2-R6-L

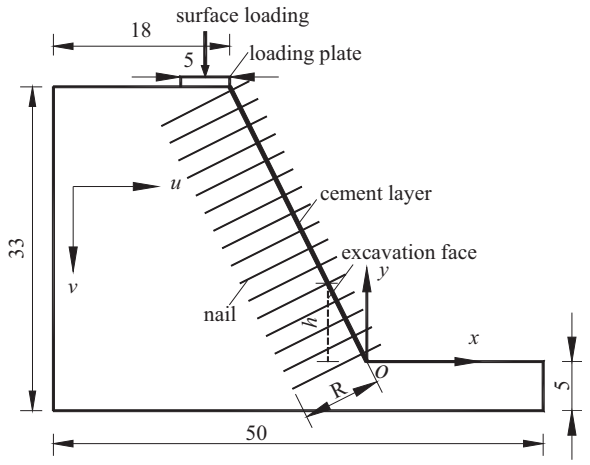

Fig. 1. Schematic views of test model under different loading conditions applied to the slope in various separate tests (unit: cm).

2.2. Model preparation

The model slope was placed in an aluminum alloy model container that was 50 cm in length, 20 cm in width, and 35 cm in height. All the slope models were 28 cm in height with a 5-cm-deep horizontal ground layer. The container sides in contact with the slope were coated with silicone. This measure, together with the ground layer, was used to diminish the influence of the model container on the slope response.

A cohesive soil with a specific gravity of 2.7 was retrieved from the soil base of a high-rise building in Beijing for use in the slope model in the tests. The liquid limit and plastic limit of the soil were 33.5% and 15.5%, respectively; indicating that the soil is a type of clay. The average particle size (d_{50}) of the clay was 0.01 mm, and particle sizes d_{10} and d_{60} of the clay were 0.001 mm and 0.02 mm, respectively. The maximum density of the clay was about 1.8 g/cm^3. The soil was

compacted to the design dry density of 1.51 g/cm^3, with a water content of 17% (i.e., saturation degree: 75%), by horizontal layer with thickness of 5–6 cm in the model container. Excess soil was then removed to form the slope model. The shear strength of the soil were determined using the consolidated-drained triaxial tests and can be described using the Mohr–Coulomb criterion, with 24° as the internal frictional angle and 26 kPa as the cohesion as the effective stress parameters.

The nail was simulated using a thin steel needle with a diameter of 1 mm in the tests. The tensile strength and the elastic modulus of the steel were 200 MPa and 210 GPa, respectively. For simplicity in model preparation, the nails were inserted orthogonally with the slope surface into the slope with a uniform distribution spacing of 2 cm. It can be concluded that the inclination of nails would have a small effect on the fundamental rules obtained in this paper. Note that the nails were arranged only in the upper part of the slope in the excavation tests because the excavation was conducted on the lower part of the slope (Fig. 1).

A new technique was developed to simulate shotcrete and the rock bolt support of the soil nail wall using a cement layer during centrifuge model tests (Fig. 2). After preparing the slope model, a type of special-made Portland cement was smeared on the slope surface with thickness of 2 mm at 1g-level (earth gravity). At this moment, the cement layer was very soft; thus the nails were then easily inserted into the slope and remained an outcrop on the slope surface with several centimeters (Fig. 2). The nails were kept vertical with the slope surface with aid of a drawing square. The cement reaches a compression strength of 15 MPa from the fully flexible state within two hours, which satisfies the simulation time requirement for soil nailing during centrifuge model tests. In other words, the cement layer reached the required strength within two hours while maintaining a centrifugal acceleration of 50g.

The friction behavior of the nail–soil interface has been investigated using a series of nail pull-out tests under different constant overburden pressures (Zhang et al., 2013). The Mohr–Coulomb criterion was found to describe the relationship between the friction stress and overburden pressure, with 16 kPa in the cohesion and 23° in the frictional angle as the effective stress parameters.

2.3. Test process

For the self-weight loading tests, the centrifugal acceleration was applied on the model by a step-wise increase of 5g. The centrifugal acceleration was maintained for a few minutes at each stage to assure the deformation of the slope resulting from the self-weight loading becoming stable. The centrifugal acceleration increment decreased to 1–2g when a slope failure was predicted to occur. The loading was ceased upon observed slope failure.

For the vertical loading and excavation tests, the centrifugal acceleration was gradually increased to 50g. The loading plate and excavation blade did not contact the slope while increasing the centrifuge acceleration. Vertical loading or excavation was conducted to the slope after the slope settlement became stable at 50g. Vertical loading was applied to the top of the slope at a rate of 1 mm/s via a loading plate with a width of 5 cm using a vertical loading device (Zhang et al., 2013) (Fig. 1). The loading device consists of an electric motor and corresponding reducer, which applies a vertical load with capacity of 10 kN on the loading plate through the shaft. Excavation was conducted near the toe of the slope using an excavation simulator (Li et al., 2011) (Fig. 1). The simulator realizes the excavation by using the steel blade, which is pushed vertically down into the slope and then cut soil away from the slope.

2.4. Measurement

The vertical load was measured using a load transducer installed on the loading plate during the vertical loading tests, and the loading pressure was obtained as the load divided by the area of the loading plate. Settlement of the loading plate was measured using a laser displacement transducer.

The images of lateral side of the slope were recorded using an image-recording and displacement measurement system during the tests (Zhang et al., 2009). The displacement history of an arbitrary point on the lateral side of the slope, where a number of white granite particles were embedded to obtain a gray-variance region required by the measurement, was determined based on an image-correlation algorithm using the captured image series (Zhang et al., 2009). In this paper, the measurement accuracy of displacement reached 0.03 mm at

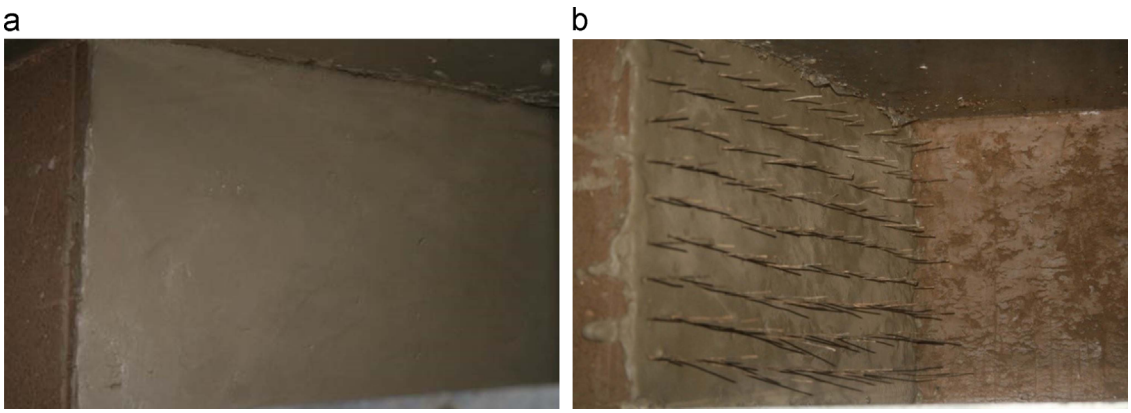

Fig. 2. Precasting of soil nail wall before tests. (a) Cement layer on the slope; (b) nails.

the model dimension. The slip surface of the slope, which appeared near the failure of the slope were directly by hand determined according to the captured images because it could be easily distinguished on the image. The Cartesian coordinate system was established with the center of the slope toe as the origin. Positive was defined as to the right in the horizontal direction (x-axis) and upward in the vertical direction (y-axis) (Fig. 1).

All measured results were presented at the model dimension in this paper. The prototype dimension of the length and measured displacements can be obtained by multiplying the model dimension of those with the centrifugal acceleration. The prototype dimension of the loading pressure was equal to the model dimensions.

3. Failure mode and limit bearing capacity

Fig. 3a shows an image of a slope at failure state under the self-weight loading condition. It can be seen that an evident slip surface appeared in the slope and that significant fracture occurred in the lower part of cement layer. The locations of the slip surface and the cement layer's fracture were easily distinguished on the image (Fig. 3a). Thus, they were determined directly by hand according to the image and drawn in Fig. 3b by outlining the nail-reinforced zone. The slip surface passed by the nails in the upper part of the slope but passed through the nails in the lower part of the slope. Similar phenomena were confirmed by observations from other tests.

Fig. 4 compares the slip surfaces of the slopes with different nail lengths and different gradients under the self-weight loading condition. The slip surface was shown to depend significantly on the nail length (Fig. 4a). For example, the slip surface moved deeply into the slope if the nail length was increased from 4 cm to 8 cm. The slip surface of the reinforced slope with a nail length of 4 cm was fairly close to that of the unreinforced slope in the middle and lower parts of the slope. This result demonstrated that the nails did not significantly affect the failure features of the slope when the nail length was relatively small. The nail length should be much longer than the maximum depth of the critical slip surface of the unreinforced slope for a better reinforcement effect. In other words, the slip surface of an unreinforced slope can be used to direct the nail design. The slip surfaces of reinforced slopes became deeper as the gradient of the slope decreased, e.g., from 5:1 to 3:1 (Fig. 4b).

Fig. 5 shows the slip surfaces of the 3:1 slope reinforced with 6-cm-long nails under the vertical loading condition. Vertical loading caused two slip surfaces that differed significantly from the slip surface induced by the self-weight loading outlined in Fig. 4. The slip surfaces nearly passed through the inner edge of the loading plate and the toe of the slope. This result demonstrated that the slip surface was controlled by the feature of the vertical load, as was confirmed in previous centrifuge model tests (Zhang et al., 2013).

Fig. 6 shows the slip surfaces of the 3:1 slope reinforced with 8-cm-long nails under the excavation condition. It can be seen that the slip surface also passed through the nail-reinforced zone.

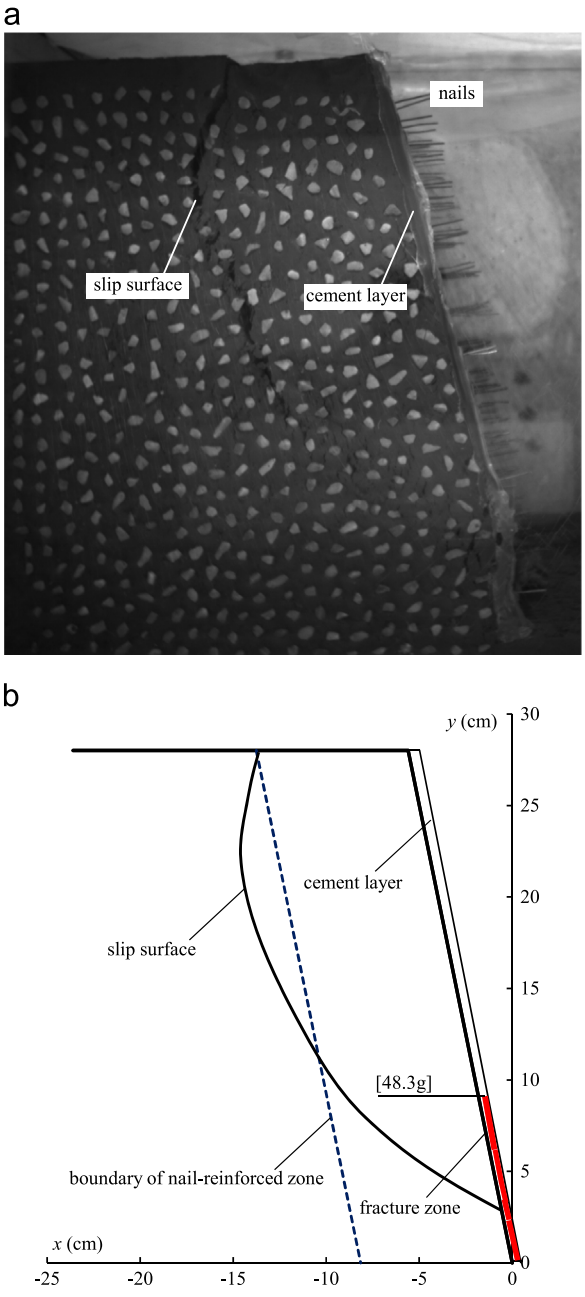

Fig. 3. Failure features of the 5:1 slope reinforced with 8-cm-long nails under self-weight loading conditions (G5-R8-S). (a) Image; (b) schematic view. Numbers in square brackets show centrifugal acceleration corresponding to fraction height of cement layer.

Close comparison showed that the slip surface depended significantly on the loading conditions (Figs. 4–6). For example, self-weight loading, which applied the volumetric force on the slope, induced the deepest slip surface compared with the other two loading conditions that apply loads on the slope surface.

To ensure a unified description of different loading types, the limit bearing capacity of a slope was defined as the load at which the slope failed, meaning that the slip surface of the slope fully appeared as determined based on the captured images. For the self-weight loading condition, the limit bearing capacity was defined based on the ultimate

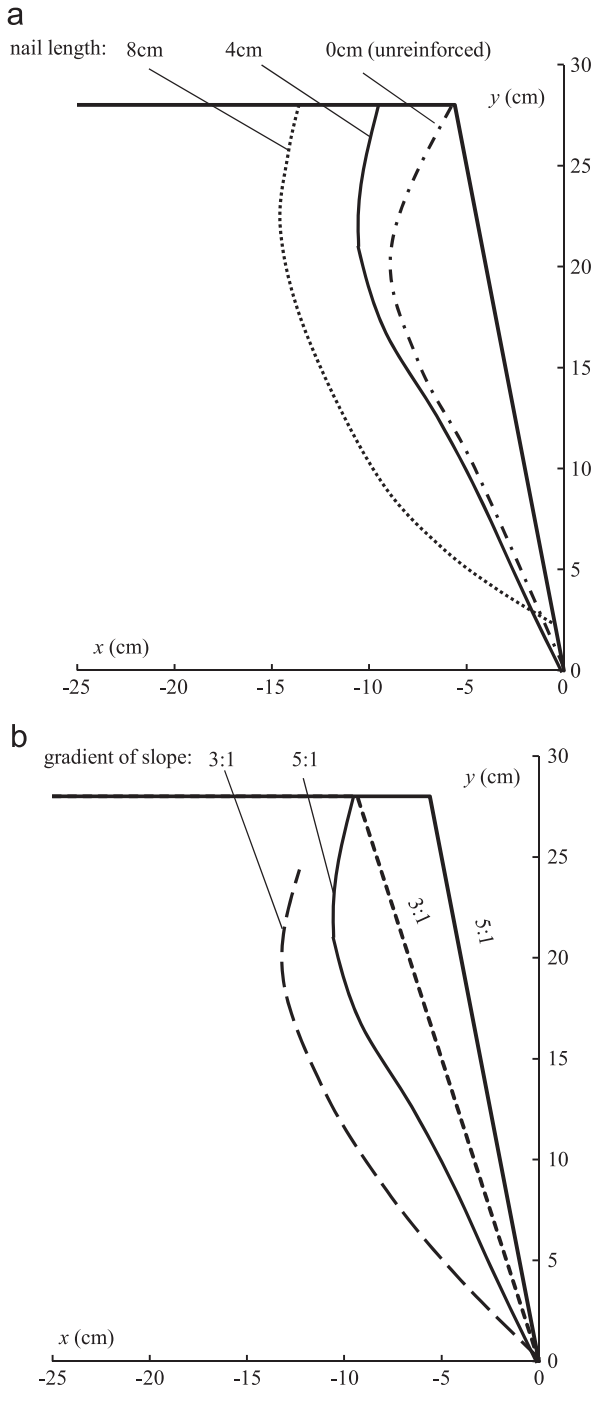

Fig. 4. Slip surfaces of slope in different self-weight loading tests. (a) varying nail lengths for the 5:1 slope; (b) varying gradients for the slope reinforced with 4-cm-long nails.

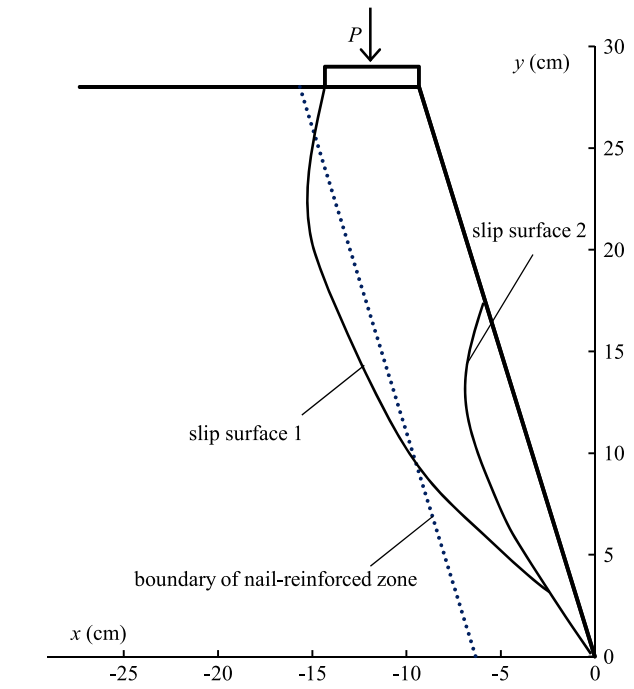

Fig. 5. Slip surface of a 3:1 slope under vertical loading conditions (G3-R6-L).

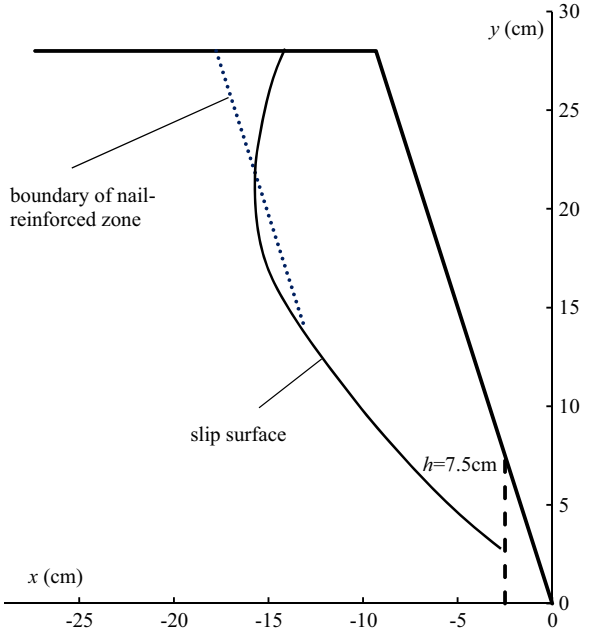

Fig. 6. Slip surface of a 3:1 slope under excavation conditions (G3-R8-E). h, excavation height.

centrifugal acceleration at which the slope failed; the ultimate centrifugal accelerations in different tests are summarized in Fig. 7. It can be inferred that as the nail length increased, small increases were observed in the limit bearing capacity for nails shorter than 4 cm in length, while more significant increases were observed when the nail length was greater than 4 cm. This was consistent with the influence rules of the nail length on the slip surface of the slope. The maximum depth of the slip surface of the unreinforced slope was approximately 3 cm, indicating that this is the benchmark depth that can be used to distinguish the reinforcement effect. Thus, it can be concluded that the nail reinforcement length should largely exceed the maximum depth of the slip surface of the unreinforced slope.

The bearing capacity of the slope failure (P_u) under the vertical loading condition was described using the ultimate loading pressure at slope failure, as shown in Fig. 8. The ultimate loading pressure was determined to be approximately equal to the stable value, or peak value, of the loading pressure

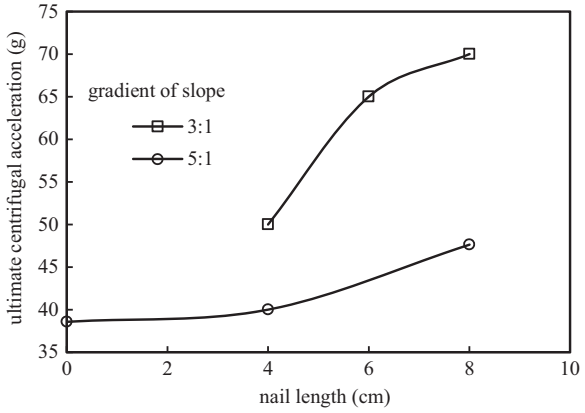

Fig. 7. Ultimate centrifugal accelerations for the slopes under self-weight loading conditions.

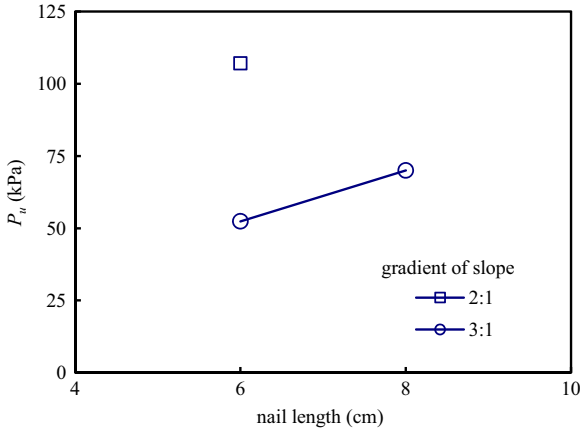

Fig. 8. Ultimate loading pressures of the slopes under vertical loading conditions. P_u, ultimate loading pressure.

in the load-settlement curves of the loading plate. It can be seen that the limit bearing capacity of the slope decreased as the nail length decreased and the slope gradient increased under the vertical loading condition. Under the excavation condition, the limit bearing capacity of the slope was described using the excavation height (h_u) at slope failure (Fig. 9). The limit bearing capacity of the slope was shown to increase with increasing nail length and with decreasing slope gradient, which was similar to other loading conditions.

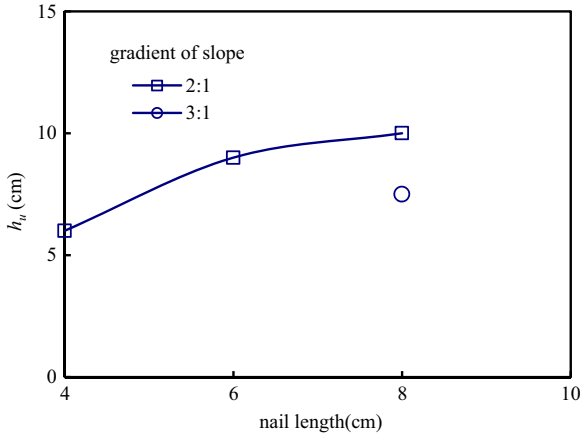

Fig. 9. Ultimate excavation heights for slopes under excavation conditions. h_u, ultimate excavation height.

4. Failure process

Close examination of captured images of reinforced slopes revealed that the slope exhibited significant failure process during loading. The full failure process of slopes reinforced using soil nailing was examined through observations in the centrifuge model tests, which included fracture of the cement layer and formation of the slip surface.

A typical fracture process of the cement layer of a reinforced slope was analyzed based on the images captured throughout the tests (Fig. 10). First, a few tiny cracks appeared in the cement layer near the toe of the slope at the 35g-level (Fig. 10a). The cracks developed with increasing centrifugal acceleration and proliferated horizontally at the 45g-level (Fig. 10b). The local failure expanded upwards in the cement layer as the centrifugal acceleration increased and a small area of the slope was crushed at the 47.6g-level (Fig. 10c). Finally, the local failure of the cement layer occurred within an area of the lower part of the slope (Fig. 10d). Thus, the images revealed that local failure of the cement layer appeared and progressively developed with the application of loading.

The appearance and development of slip surface of the slope was analyzed on the basis of the relative displacement of point couples on opposite sides of the slip surface, selected with a spacing of 10 mm. Fig. 11 shows the point couples for analysis of a typical reinforced slope. Their relative displacements under self-weight loading conditions, tangential and normal to the slip surface, were obtained using image-based measurements (Fig. 12). The relative displacements of all the point couples were found to increase with increasing centrifugal acceleration. For every point couple, the tangential relative displacement was larger than the normal relative displacement at a given centrifugal acceleration, demonstrating that the slippage failure occurred along the slip surface. In all cases, the tangential relative displacement increased slowly with increasing centrifugal acceleration, followed by a remarkable inflection in each of the history curves, after which the tangential relative displacement increased significantly as the centrifugal acceleration increased. Such an inflection can be regarded as an indicator of the appearance of slippage failure in the slope. The inflection can be accurately determined as the intersection of tangents to the history curve near the inflection, as indicated by the dashed line in Fig. 12. This phenomenon allowed clear determination of the centrifugal accelerations at which the local slippage appeared along the slip surface.

Fig. 11 identifies the centrifugal accelerations at which local failures occurred to describe the development process of the slip surface under the self-weight loading condition. The local failure first appeared near the toe of the slope and it gradually developed upwards until finally reaching the top of the slope. This result demonstrated that the nail-reinforced slope underwent a significant failure process. The area of the cement layer

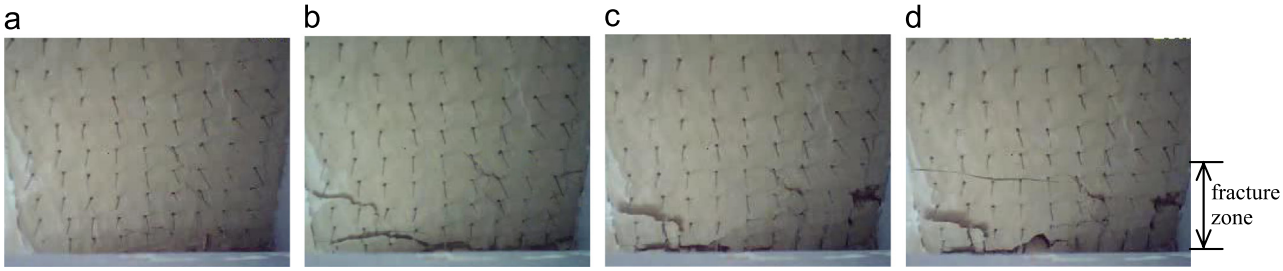

Fig. 10. Fracture process of the cement layer of 5:1 slope with 8-cm-long nails under self-weight loading conditions (G5-R8-S). (a) 35*g*; (b) 45*g*; (c) 47.6*g*; (d) 48.3*g*.

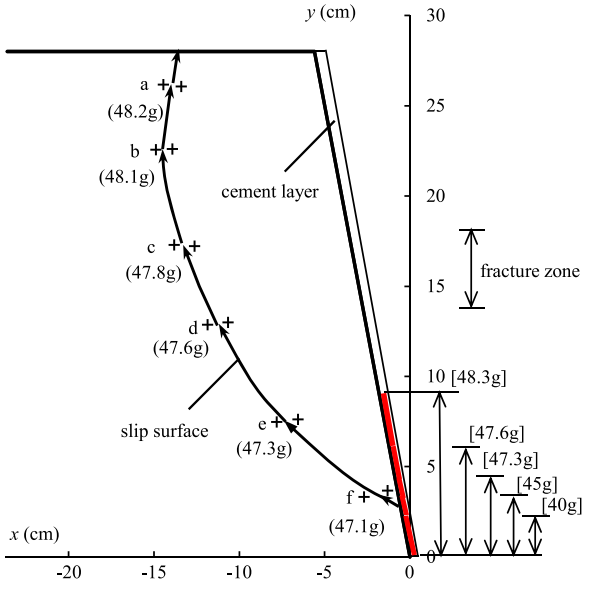

Fig. 11. Failure process of 5:1 slope with 8-cm-long nails under self-weight loading conditions (G5-R8-S). Arrow, direction of the failure sequence; numbers in round bracket and square bracket, centrifugal accelerations that indicate the appearance of local failure and fraction zone height of the cement layer, respectively.

fracture is also outlined at different centrifugal accelerations in Fig. 11. The cement layer was observed to exhibit a fracture prior to the occurrence of the slip surface, demonstrating that the cement layer fracture, which reduced the restriction of the cement layer on the slope, was an important prerequisite for slippage failure of the slope. The slippage failure of the slope caused a significant movement of the slippage body, in turn aggravating the cement layer fracture. Therefore, the slippage failure of the slope and fracture of the cement layer developed with a coupling effect until the final landslide occurred.

Comparison of the local failure sequences of slopes indicated that the slip surface developed gradually from the toe of the slope upwards to the top of the slope for all the tests under self-weight loading conditions (Fig. 13). This result demonstrated that the failure sequence was not influenced by the length of the nail or the gradient of the slope, but instead depended primarily on the loading condition. For the unreinforced and 4-cm-long nail-reinforced slopes with a gradient of 5:1, local tension failure occurred near the top of the slope, which was determined because the normal relative displacement was larger than the tangential relative displacement at the point couples. However, local slippage failure occurred at this location when reinforcement nails of adequate length were used (e.g., 8 cm). This result demonstrated that use of the nailing changed the failure properties of the slope, which restricted the tension crack in the slope.

Fig. 14 shows the failure sequence of a reinforced slope under vertical loading conditions that was investigated via point couple analysis. The failure sequence was shown to be a relatively more complex process compared with the self-weight loading conditions. The vertical load first induced local slippage near the toe of the slope and at the inner edge of the loading plate. These local slippages extended to the interior of the slope and eventually developed into a full slip surface. Similar failure sequences under vertical loading conditions have been demonstrated in centrifuge model tests on nail-reinforced slopes without cement layers (Zhang et al., 2013).

Fig. 15 shows the failure processes of different reinforced slopes under excavation conditions. The slip surface first occurred near the toe of the slope and then developed upwards to the top of the slope. Whereas the nail length did not affect this pattern of slip surface development, it was shown to influence the local failure properties of the slope, similar to the self-weight loading condition results (Fig. 13). For example, local tension failure appeared near the top of slope with a nail length of 4 cm, but this changed to slippage failure at nail lengths of 6 cm and 8 cm.

In summary, the reinforced slopes underwent significant failure processes that were influenced by both the loading conditions and reinforcement arrangements. Stability analysis methods should capture the features of such a failure process.

5. Failure process mechanism

5.1. Deformation-based analysis

The failure process mechanism of the reinforced slope was analyzed on the basis of the deformation behaviors observed via image-based measurements. Fig. 16 shows a series of horizontal displacement contours of a reinforced slope at different loads under self-weight loading conditions. Significant horizontal displacement was observed at the 35*g*-level (Fig. 16a). The contour lines of horizontal displacement exhibited a tendency of concentration, demonstrating significant deformation localization near the toe of the slope as the centrifugal acceleration increased to the

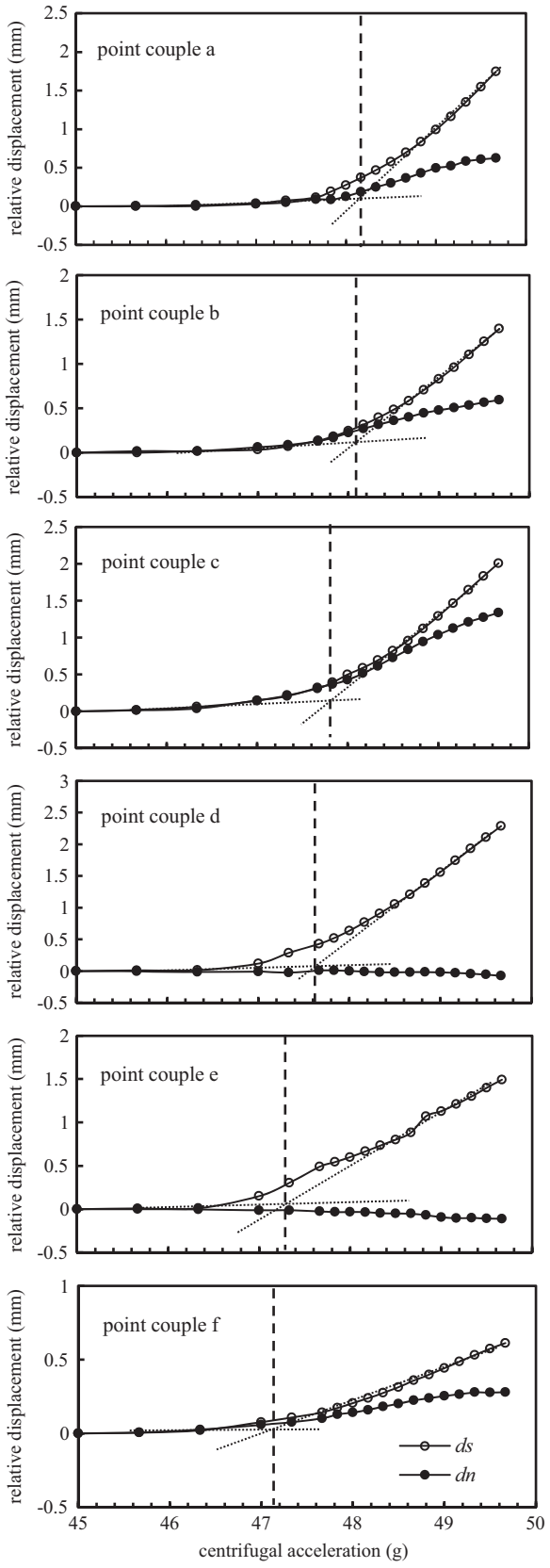

Fig. 12. Histories of relative displacement of point couples of a 5:1 slope with 8-cm-long nails under self-weight loading conditions at model dimension (G5-R8-S). *ds* and *dn*, relative displacements tangential and perpendicular to the slip surface, respectively.

45*g*-level (Fig. 16c). This localized deformation caused the nearby cement layer to crack because the cement was unable to bear such a significant non-uniform deformation (Fig. 10b). The extent of deformation localization near the toe of the slope

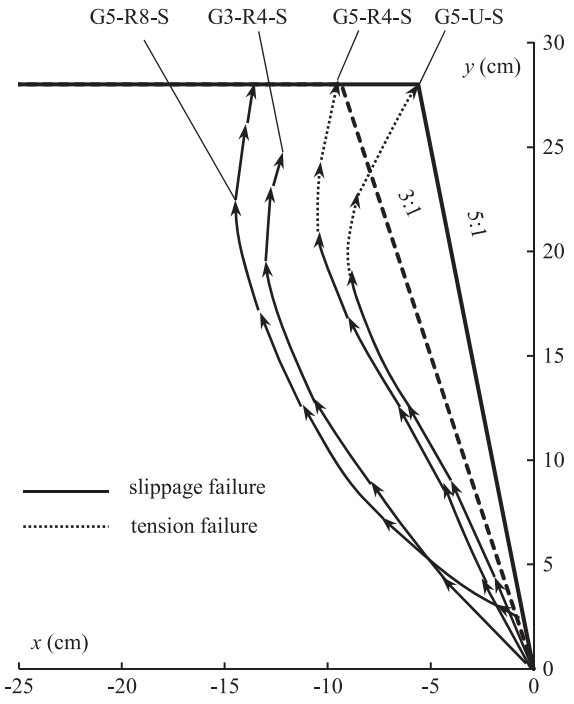

Fig. 13. Failure processes of slopes in different self-weight loading tests. arrow, direction of the failure sequence.

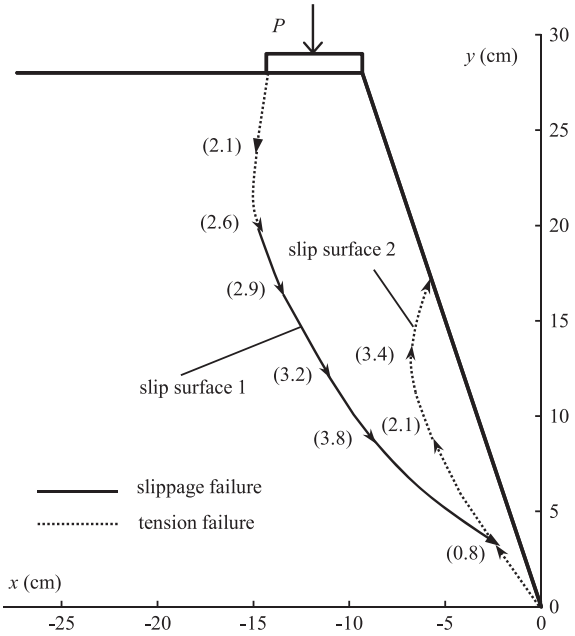

Fig. 14. Failure process of 3:1 slope with 6-cm-long nails under vertical loading conditions (G3-R6-L). Arrow, direction of failure sequence; number in bracket, settlement (unit: mm) of loading plate corresponding to the appearance of slippage.

increased following the rupture of the cement layer, and the zone with the localized deformation developed upwards to the top of the slope with increasing centrifugal acceleration (Fig. 16d–g). The development of the deformation localization zone was shown to be similar to the failure sequence of the reinforced slope. This implied that the deformation localization within the slope was the primary driver of the slope failure process and can therefore be used to analyze the failure mechanism of the slope.

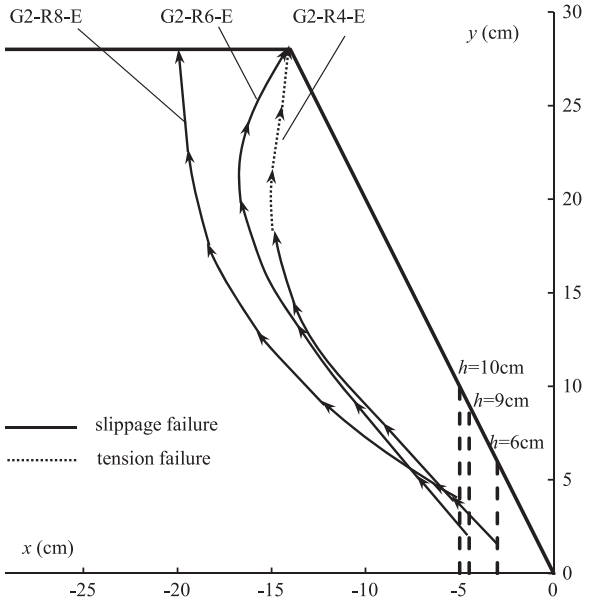

Fig. 15. Failure sequence of 2:1 slopes in excavation tests. h, excavation height; arrow, direction of the failure sequence.

Fig. 17a shows the horizontal distribution of the horizontal displacement of a reinforced slope at several elevations at different g-levels. The horizontal displacement increased monotonically from the interior to the surface of the slope. Before the centrifugal acceleration approached the range at which the failure of the slope occurred, a segment can be observed with significant gradient along the horizontal distribution curve of the horizontal displacement, indicating significant deformation localization there. The gradient of the horizontal displacement, defined as the ratio of the increment of displacement to the increment of x-coordinate, was used to quantify the extent of the deformation localization (Fig. 17b). Fig. 17b shows that the gradient of horizontal displacement was fairly small across the entire slope at the 40g-level and increased significantly with an evident peak value as centrifugal acceleration increased to the 45g-level. At that point, the gradient of horizontal displacement around the location of the peak was significantly larger than in other locations, which demonstrates that a deformation localization zone was induced in the slope by the self-weight loading. After the deformation localization zone appeared, the gradient of horizontal displacement in the deformation localization zone increased at a significantly more rapid rate than in other areas during the loading process. The slip surface that ultimately appeared in the zone is outlined with dashed lines in Fig. 17b, it was denoted g-level based on the analytical results of the failure process shown in Fig. 11. The slip surface was found to appear after, and is therefore inferred to result from, the occurrence of a localized deformation zone. Close examination showed that the deformation localization zone moved from the interior to the surface of the slope with decreasing elevation from the top of

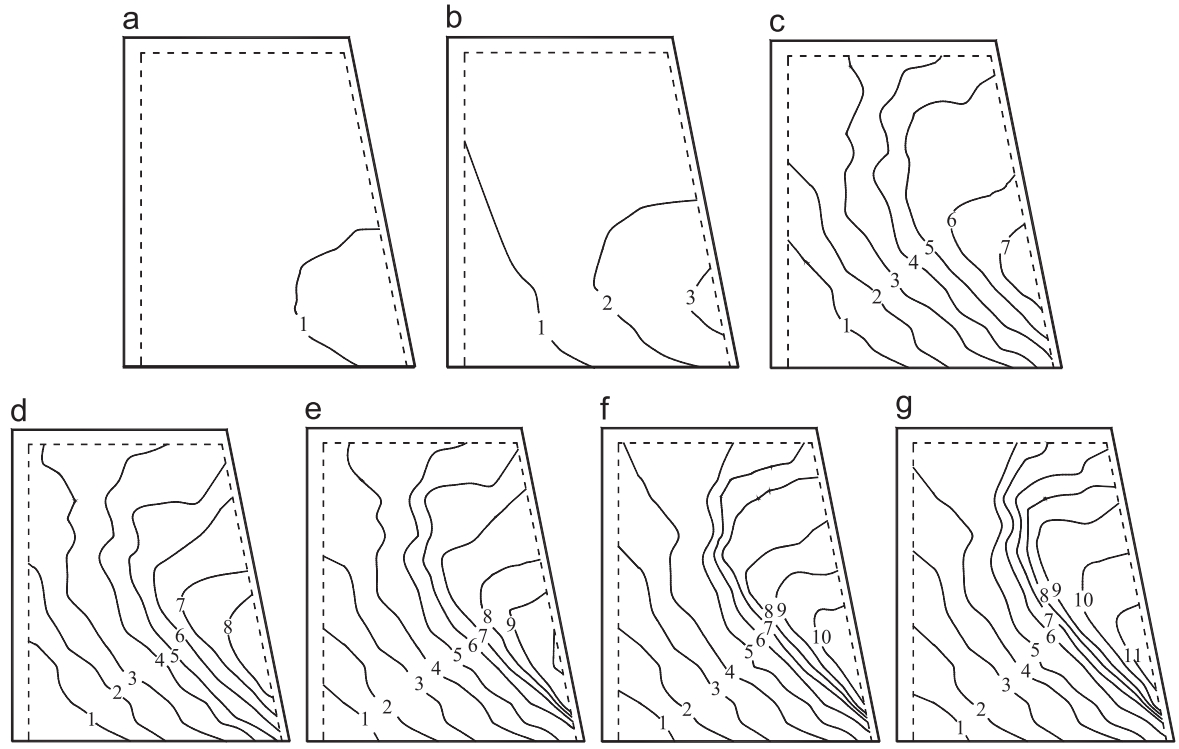

Fig. 16. Horizontal displacement contours of the 5:1 slope with 8-cm-long nails in self-weight loading test at model dimension (G5-R8-S) (unit: mm). (a) 35g; (b) 40g; (c) 45g; (d) 45.7g; (e) 46.3g; (f) 47g; (g) 47.7g.

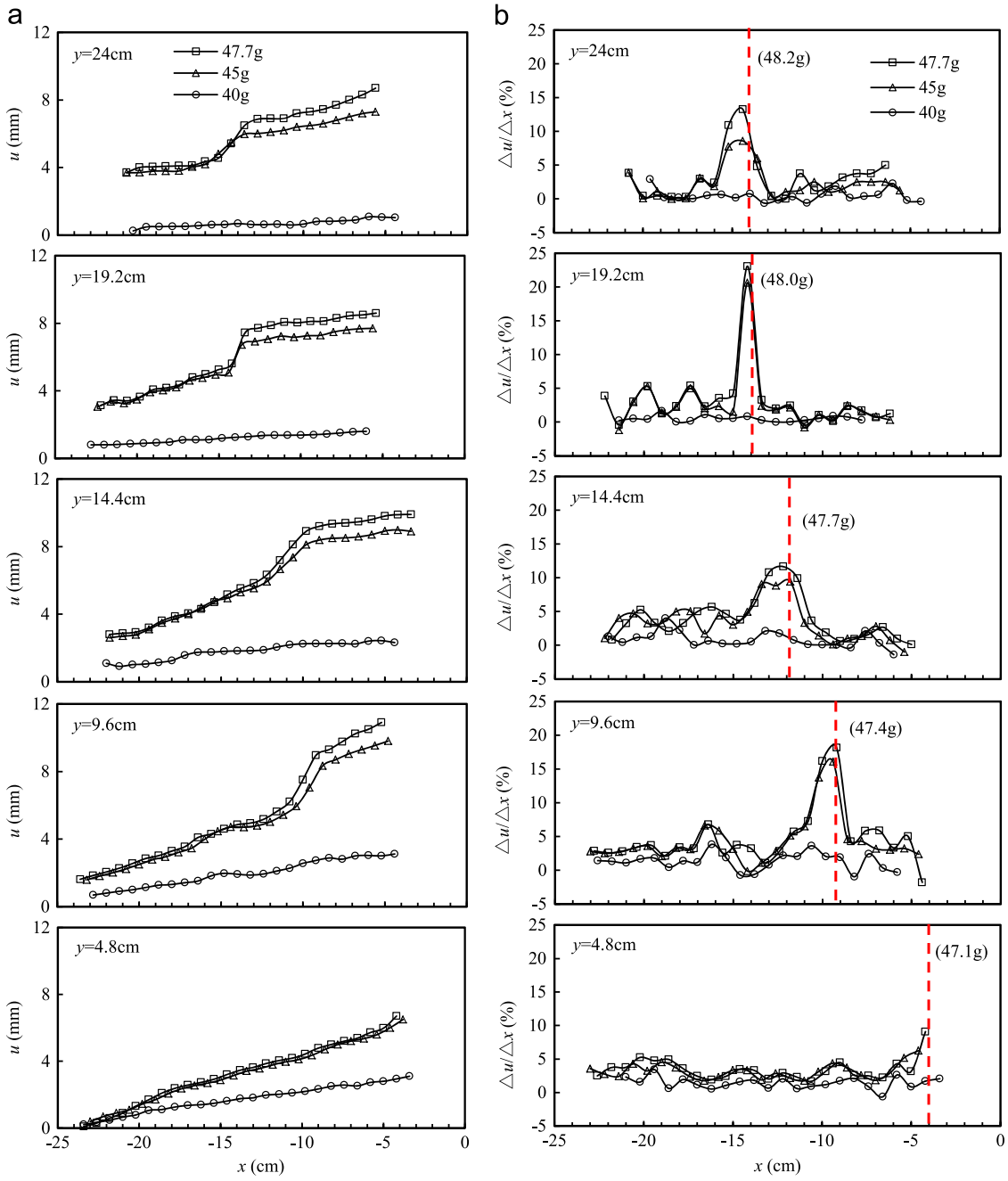

Fig. 17. Horizontal distributions of horizontal displacement of 5:1 slope with 8-cm-long nails in self-weight loading test at model dimension (G5-R8-S). (a) Horizontal displacement; (b) gradient of horizontal displacement. u, horizontal displacement; $\Delta u/\Delta x$, gradient of horizontal displacement; dashed line, location of slip surface; number in round bracket, centrifugal accelerations that indicate the appearance of local failure.

the slope, which was consistent with the shape of the final slip surface. Therefore, it can be concluded that the deformation localization was induced by the loading and ultimately resulted in the development of the slip surface. The slip surface can be estimated using the deformation localization zone prior to slope failure.

5.2. Reinforcement mechanism

The nail reinforcement mechanism can be explained via the deformation-based analysis. The distributions of the gradient of horizontal displacements of the unreinforced slope showed similar tendency as the reinforced slopes, although the deformation localization zone appeared earlier (Fig. 18). This indicated that both the reinforced and unreinforced slopes are driven by the same failure mechanism. The use of a soil nailing significantly decreased the slope deformation and subsequently delayed the occurrence of the deformation localization within the slope, therefore arresting the failure of the slope. This conclusion was confirmed by the observations in other groups of centrifuge model tests with varied slope gradients and loading conditions.

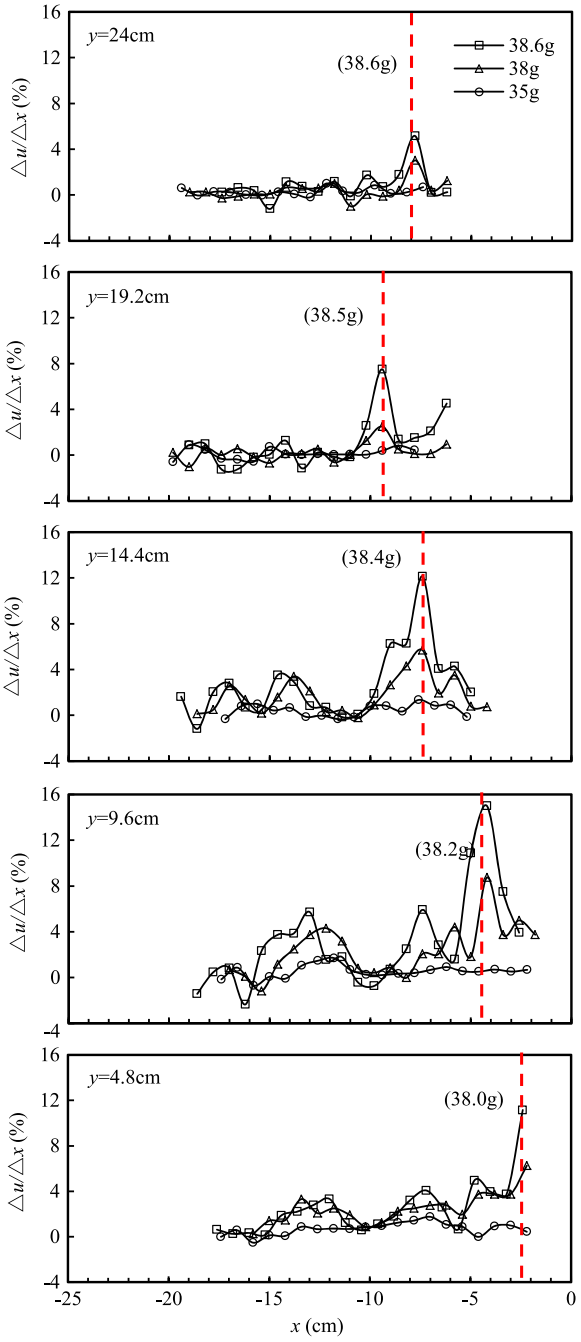

Fig. 18. Horizontal distributions of gradient of horizontal displacement of 5:1 unreinforced slope in self-weight loading test at model dimension (G5-U-S). $\Delta u/\Delta x$, gradient of horizontal displacement; dashed line, location of slip surface; number in round bracket, centrifugal accelerations that indicate the appearance of local failure.

5.3. Nail responses

The nails were examined after the tests. The results showed that the nails did not break due to tension and exhibited evident flexural deformation near the slip surface. Pull-out deformation of nails was inferred but could not be measured accurately. Note that, despite experiencing significant bending, nails still passed through the slip surface over a large area in the slope. This result indicated that the failure analysis of slopes reinforced with soil nailing should consider not only nail pull-out but also nail bending deformation as well as their combination. In other words, both types of nail failure mechanisms, including pull-out failure and bending deformation, and their combination need to be analyzed to evaluate their effect on stability of a reinforced slope.

The nail deflections, which described the bending deformation and reflect the complicated nail–soil interaction, can be obtained directly from the corresponding displacement of soil that was measured using the image-based analysis. The validity of this method has been preliminarily verified in previous studies (Zhang et al., 2013).

The distributions of nail deflections at different locations were determined and described along the nail using a local w–X coordinate system under different loading conditions (Fig. 19). In the local w–X coordinate system, the X-axis and w-axis were defined as parallel to the nail and the slope surface, respectively; this is depicted in Fig. 19a along with the positive direction of the coordinate axes and the location of measurement nails. Note that the deflection of nails was only presented in upper part of slope for the excavation tests because the nails were limited to those locations (Fig. 19b). The deflections of nails increased during loading, reflecting an increase in nail–soil interaction due to application of loading. The distribution of nail deflections exhibited different characteristics in different locations (Fig. 19b–d). For example, under self-weight loading conditions, the deflection of the nail in upper part of the slope increased from the interior of the slope, whereas it was nearly a parabola with a peak value near the slope surface in the lower part of the slope (Fig. 19c). On the other hand, the loading conditions had a significant effect on the distribution of nail deflection. The vertical loading induced a nearly contrary rule in the distribution of deflection compared with the self-weight loading condition. A parabolic distribution curve was observed in the upper part of the slope, with a monotonic increase in the lower part of the slope (Fig. 19d). The distribution of nail deflection was similar for both the vertical loading and excavation conditions (Fig. 19b and d).

6. Conclusions

A series of centrifuge model tests was conducted on the slopes reinforced with soil nail wall under three types of loading conditions: a self-weight loading applied with a volumetric force, and a vertical loading and excavation applied to different types of surface loads on the slope. Image-based observation and measurements of the slope, nails, and cement layer were used to study the behavior and mechanism of failure process of reinforced slopes. The main conclusions drawn are as follows:

(1) The soil nailing significantly increased the stability level and restricted the tension cracks of the slopes. Increasing the nail length improved the stability of reinforced slopes with deeper slip surfaces.
(2) The reinforced slope exhibited a significant failure process during loading. The slippage failure of the slope and

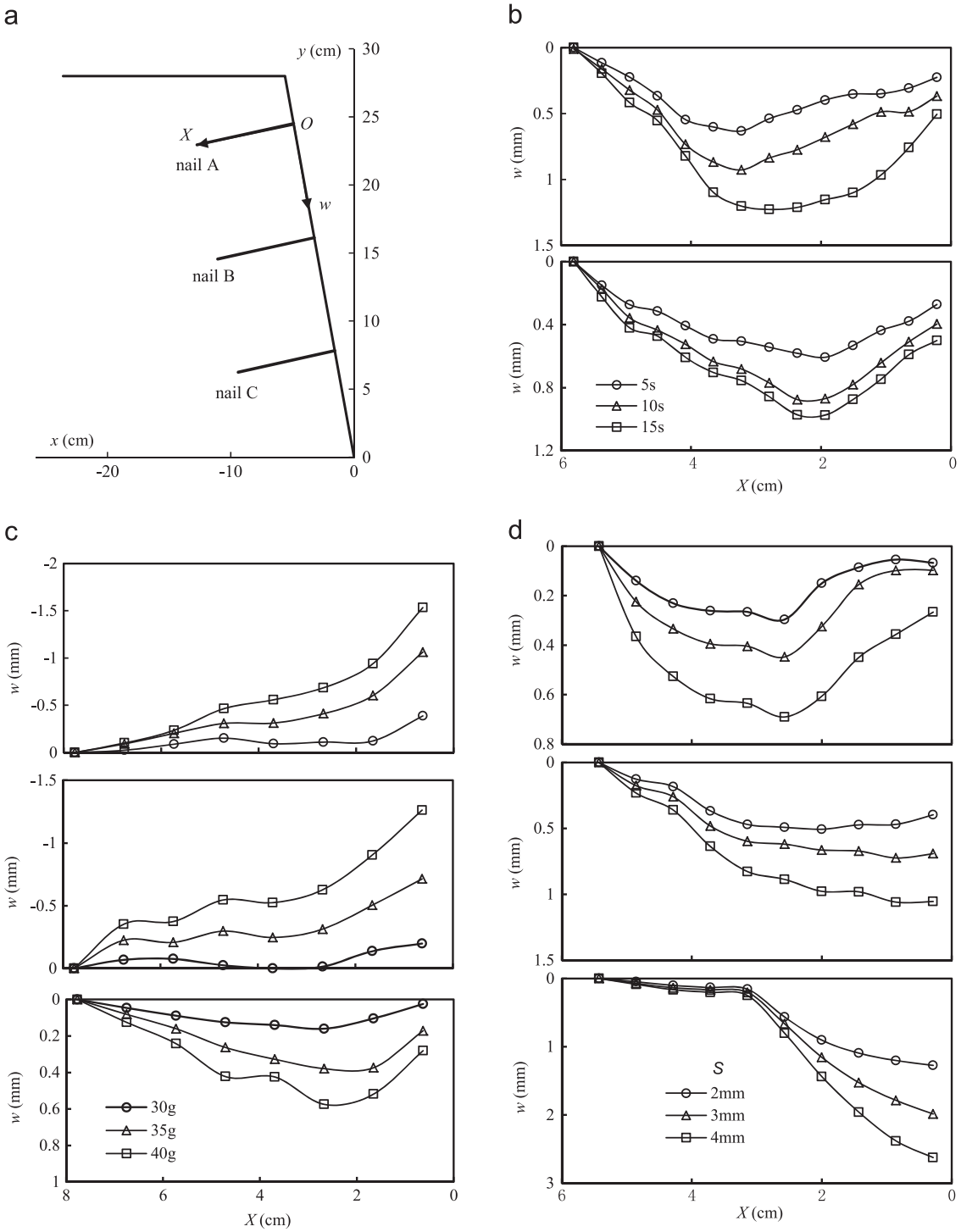

Fig. 19. Distributions of nail deflections of reinforced slopes at model dimension in different tests. (a) Locations of measurement nails; (b) 2:1 slope with 6-cm-long nails under excavation conditions (G2-R6-E); (c) 5:1 slope with 8-cm-long nails under self-weight loading conditions (G5-R8-S); (d) 3:1 slope with 6-cm-long nails under vertical loading conditions (G3-R6-L). *w*, nail deflection; *X*, distance from slope surface.

fracture of the cement layer developed in turn with a coupling effect until final landslide occurred.

(3) The deformation localization was induced by loading within the slope and ultimately developed into a slip surface. Slope failure features, such as the slip surface, can therefore be estimated according to the deformation localization zone. Similarly, the reinforcement mechanism of the nailing can be described using the deformation localization zone: the soil nailing significantly reduced the deformation of the slope, and accordingly delayed the occurrence of the deformation localization.

(4) The nails exhibited increasing deflections with different distributions in different locations of slope during loading. Nail failure was recognized as a combination of pull-out failure and bend deformation.

(5) Slope deformation and nail deflection were significantly dependent on the loading conditions. Consequently, the loading condition had a large effect on the slip surface with the formation sequence and on the features of soil–nail interaction. Self-weight loading induced a failure process from the toe to the top of the slope; while vertical loading and excavation caused failure sequences that are opposite to one another and have a relatively shallow slip surface.

It should be noted that the centrifuge model tests used only a type of cohesive soil and inadequately considered different physical state of the soil. For example, the saturated slopes may exhibit more complicated response near failure due to effect of pore pressure. Therefore, the conclusions should be carefully applied in the real soil nail wall design. Systematic investigations which consider more factors are expected to be conducted in a future study based on the findings of this study.

Acknowledgements

The study is supported by the State Key Laboratory of Hydroscience and Engineering (no. 2014-KY-1), National Program for Support of Top-notch Young Professionals, and National Natural Science Foundation of China (no. 51479096).

References

Andrzej, S., Danuta, L., Marek, K., 1988. Measured and predicted stresses and bearing capacity of a full scale slope reinforced with nails. Soils Found. 28 (4), 47–56.

Cheuk, C.Y., Ng, C.W.W., Sun, H.W., 2005. Numerical experiments of soil nails in loose fill slopes subjected to rainfall infiltration effects. Comput. Geotech. 32, 290–303.

Fan, C.C., Luo, J.H., 2008. Numerical study on the optimum layout of soil–nailed slopes. Comput. Geotech. 35, 585–599.

Gui, M.W., Ng, C.W.W., 2006. Numerical study of a nailed slope excavation. Geotech. Eng. 37 (1), 1–12.

Guler, E., Bozkurt, C.F., 2004. The effect of upward nail inclination to the stability of soil nailed structures. Geotech. Eng. Transp. Projects, 2213–2220.

Junaideen, S.M., Tham, L.G., Law, K.T., Lee, C.F., Yue, Z.Q., 2004. Laboratory study of soil–nail interaction in loose, completely decomposed granite. Can. Geotech. J. 41, 274–286.

Juran, I., Baudrand, G., Farrag, K., Elias, V., 1990. Kinematical limit analysis of soil–nailed structures. J. Geotech. Div. ASCE 116 (1), 54–73.

Kim, J.S., Kim, J.Y., Lee, S.R., 1997. Analysis of soil nailed earth slope by discrete element method. Comput. Geotech. 20 (1), 1–14.

Li, M., Zhang, G., Zhang, J.M., Lee, C.F., 2011. Centrifuge model tests on a cohesive soil slope under excavation conditions. Soils Founda. 51 (5), 801–812.

Nowatzki, E., Samtani, N., 2004. Design, construction, and performance of an 18-meter soil nail wall in Tucson, AZ. Geotech. Spec. Publ. ASCE 124, 741–752.

Patra, C.R., Basudhar, P.K., 2005. Optimum design of nailed soil slopes. Geotech. Geol. Eng. 23, 273–296.

Shen, C.K., Bang, S., Hermann, L.R., 1981. Ground movement and analysis of earth support system. J. Geotech. Div. ASCE 107 (12), 1609–1624.

Tatsuoka, F., Muñoz, H., Kuroda, T., Nishikiori, H., Soma, R., Kiyota, T., Tateyama, M., Watanabe, K., 2012. Stability of existing bridges improved by structural integration and nailing. Soils Found. 52 (3), 430–448.

Turner, J.P., Jensen, W.G., 2005. Landslide stabilization using soil nail and mechanically stabilized earth walls: case study. J. Geotech. Geoenviron. Eng. 131 (2), 141–150.

Wang, L.P., Zhang, G., Zhang, J.M., 2010. Nail reinforcement mechanism of cohesive soil slopes under earthquake conditions. Soils Found. 50 (4), 459–469.

Wei, W.B., Cheng, Y.M., 2010. Soil nailed slope by strength reduction and limit equilibrium methods. Comput. Geotech. 37, 602–618.

Wong, I.H., Low, B.K., Pand, P.Y., 1997. Field performance of soil wall in residual soil. J. Perform. Constr. Facil. 11 (3), 105–112.

Yang, M.Z., Drumm, E.C., 2000. Numerical analysis of the load transfer and deformation in a soil nailed slope. Geotech. Spec. Publ. ASCE 96, 102–116.

Zhang, G., Cao, J., Wang, L.P., 2013. Centrifuge model tests of deformation and failure of nailing-reinforced slopes under vertical surface loading condition. Soils Found. 53 (1), 117–129.

Zhang, G., Hu, Y., Zhang, J.M., 2009. New image analysis-based displacement-measurement system for geotechnical centrifuge modeling tests. Measurement 42 (1), 87–96.

Zhang, J., Pu, J., Zhang, M., Qiu, T., 2001. Model tests by centrifuge of soil nail reinforcements. J. Test. Eval. 29 (4), 315–328.

Zhou, W.H., Yin, J.H., 2008. A simple mathematical model for soil nail and soil interaction analysis. Comput. Geotech. 35, 479–488.

Zhou, Y.D., Cheuk, C.Y., Tham, L.G., 2009. Numerical modeling of soil nails in loose fill slope under surcharge loading. Comput. Geotech. 36, 837–850.

Zornberg, J.G., Mitchell, J.K., Sitar, N., 1997. Testing of reinforced slopes in a geotechnical centrifuge. Geotech. Test. J. 20, 470–480.